Derivation of vertical wavelengths of gravity waves in the MLT-region from multispectral airglow observations

Carsten Schmidt[a,*], Tim Dunker[b,c], Sabrina Lichtenstern[d], Jürgen Scheer[e], Sabine Wüst[a], Ulf-Peter Hoppe[b] and Michael Bittner[a,f]

[a]German Aerospace Center (DLR-DFD), 82234 Wessling, Germany

[b]Department of Physics and Technology, UiT The Arctic University of Norway, Postboks 6050 Langnes, 9037 Tromsø, Norway,

[c]present address: Time and frequency metrology, National laboratory, Justervesenet, Postboks 170, 2027 Kjeller, Norway

[d]formerly German Aerospace Center (DLR-DFD), 82234 Wessling, Germany

[e]Instituto de Astronomía y Física del Espacio, CONICET, CC67, Suc. 28, Buenos Aires, Argentina

[f]Augsburg University (UNA), 86135 Augsburg, Germany

[*]**Corresponding Author**: Carsten Schmidt

Contact details of corresponding author:

Carsten Schmidt

German Aerospace Center

German Remote Sensing Data Center

82234 Wessling

Germany

Telephone: +49 8153 28 1335

Telefax: +49 8153 28 1363

e-mail: carsten.schmidt@dlr.de

Abstract

We present a new method for the derivation of gravity wave vertical wavelengths from OH airglow observations of different vibrational transitions. It utilizes small phase shifts regularly observed between the OH(3-1) and OH(4-2) intensities in the spectra of the GRIPS (GRound-based Infrared P-branch Spectrometer) instruments, which record the OH airglow emissions in the wavelength range from 1.5µm to 1.6µm simultaneously. These phase shifts are interpreted as being due to gravity waves passing through the OH airglow layer and affecting individual vibrational transitions at slightly different times due to small differences in their emission heights.

The results are compared with co-located observations of the OH(6-2) and O_2b(0-1) transitions by means of spectrometer observations (TANGOO instrument, Tilting-filter spectrometer for Atmospheric Nocturnal Ground-based Oxygen & hydrOxyl emission measurements) performed from 2013 until 2016 at Oberpfaffenhofen (48.08° N, 11.27° E), Germany, and with Na-Lidar measurements acquired between 2010 and 2014 at the Arctic Lidar Observatory for Middle Atmosphere Research (ALOMAR, 69.28° N, 16.01° E), Norway. The latter comparison shows best agreement if the mean height difference of the OH(3-1) and OH(4-2) emission is assumed to be 540 m (1σ=160 m), confirming the result of von Savigny et al. (2012), who derived a height difference of approximately 500 m between each vibrational level. For approximately 40 % of all wave events observed with GRIPS, a quantitative estimate of the phase relationship between the OH(3-1) and OH(4-2) intensities can be retrieved from the spectra allowing derivation of vertical wavelengths. The retrieval performs best for wave periods below two hours (80 % success rate) and worse for periods above ten hours (successful in less than 10 % of the cases). The average wavelength determined from 102 events amounts to 22.9 km (1σ: 9.0 km).

Keywords: airglow; MLT region; atmospheric gravity waves; vertical wavelengths; NDMC

1 Introduction

Airglow spectroscopy has proven to be a powerful technique for studying dynamical features of the upper mesosphere / lower thermosphere (MLT region). It is a well-established observation technique, providing a high temporal resolution as well as a high degree of reliability and stability, making it suited for instance for long-term studies (see, e.g., Bittner et al. 2000, 2002; Beig et al., 2003; French and Klekociuk, 2011; Perminov et al., 2014). On shorter time scales, especially atmospheric gravity waves and solar tides can perturb the emissions of the various airglow emissions (among others: Hines and Tarasick, 1987; Swenson and Gardner et al., 1998; López-Gonzáles et al., 2005; Wachter et al., 2015; Hannawald et al., 2016; Sedlak et al., 2016; Wüst et al., 2016; Silber et al., 2017; Wüst et al., 2017a).

The different vibrational bands of the hydroxyl (OH) molecule represent the most intensively studied airglow emission of the MLT region. Currently, 85 % of the spectrometers or photometers listed in the database of the Network for the Detection of Mesospheric Change (NDMC, http://wdc.dlr.de/ndmc) observe at least one of the various OH emissions.

While Baker and Stair (1988) are usually cited for attributing the peak height of the emitting layer to 87 km, recent studies by von Savigny et al. (2012) and von Savigny and Lednyts'kyy (2013) have shown that OH emissions from different vibrational transitions originate from slightly different altitudes. As was pointed out by von Savigny et al. (2012), these differences had already been discussed in older publications such as López-Moreno et al. (1987) and even Baker and Stair (1988). In addition to their large set of ENVISAT/SCIAMACHY (ENVironmental SATellite, Scanning Imaging Absorption spectroMeter for Atmospheric CHartographY) observations comprising OH(8-3), OH(6-2) and OH(3-1) vertical volume emission rate profiles, von Savigny et al. (2012) explain the observations via sophisticated model simulations. According to their study, peak emission altitudes of adjacent upper

vibrational levels of OH are on average separated by approximately 500 m, with higher vibrational transitions originating at higher altitude, which is mainly attributable to the altitude dependent atomic oxygen quenching rate.

This implies that atmospheric waves travelling through the OH emission layer from above or below influence the individual emissions at different points in time. Since the peak altitude differences are rather small compared to the emission layer width of approximately 8 km to 10 km, the expected signal will be small as well. However, if such a signal can be identified, it will involve information on the wave propagation direction as well as its vertical wavelength. In combination with the horizontal wavelength and the background wind, the vertical wavelength is essential in estimating the vertical energy and momentum flux (see, e.g., Swenson and Liu, 1998). Whereas estimating horizontal wavelengths from airglow imagers can be considered a straight-forward approach, deriving vertical wavelengths is a more difficult task. Complementary observations by lidars or radars do provide values for vertical wavelengths. But these instruments are rather expensive and technically complex. Therefore, such measurements are available for a few sites, only.

In the past, several approaches have been developed to derive vertical wavelengths from airglow observations. On the one hand, it is more or less self-evident to utilize different airglow emissions, such as OH, which is supposed to be representative for 86–88 km, and O_2 or OI, which represent altitudes of 94–96 km and 95–97 km. On the other hand, more sophisticated methods have been developed by Hines and Tarasick (1987), Tarasick and Hines (1990), Swenson and Gardner (1998), which retrieve information about the vertical wavelength of a gravity wave from just one emission. The latter methods take advantage of the fact that rotational temperatures derived from the vibrational transition lines are representative for a slightly different altitude than the emissions themselves and thus variations of airglow intensities and related temperatures often show a distinct phase shift in

100 the presence of propagating waves. Both methods have advantages and disadvantages, but are
101 widely used throughout the airglow community for estimating vertical wavelengths (among
102 others: Reisin and Scheer, 1996; Reisin and Scheer, 2001; López-González et al., 2005; Taori
103 et al., 2005; Guharay et al., 2008; Takahashi et al., 2011).

104 In the present study we exploit the possibility to deduce vertical wavelengths from
105 simultaneous observations of different OH vibrational transitions, namely the OH(3-1) and
106 OH(4-2) emission. The results are compared with a) co-located temperature profiles acquired
107 with the Na-lidar at the Arctic Lidar Observatory for Middle Atmosphere Research
108 (ALOMAR, 69.28° N, 16.01° E), Norway and b) co-located observations of OH(6-2) and
109 O_2b(0-1) airglow emissions at Oberpfaffenhofen (48.08° N, 11.27° E), Germany, derived
110 from ground-based observations of the TANGOO-instrument (Tilting-filter spectrometer for
111 Atmospheric Nocturnal Ground-based Oxygen & hydrOxyl emission measurements).

112 The paper is structured as follows. Section 2 describes important features of the
113 instrumentation and of the data retrieved. The results of the GRIPS/lidar and
114 GRIPS/TANGOO intercomparison are presented and discussed in section 3. We conclude
115 with a short summary and potential applications in future studies in section 4.

116

117

118 ## 2 Instrumentation

119 ### 2.1 Airglow spectrometers

120 The GRound-based Infrared P-branch Spectrometers (GRIPS) primarily observe the P-branch
121 of the OH(3-1)-rotational vibrational transition. The resolving power ($\lambda/\Delta\lambda$) of ~500 only
122 allows derivation of the rotational temperatures from their P_1 lines. On the other hand, the
123 instruments cover the spectral range from approximately 1.5 μm to 1.6 μm. Therefore, both
124 Q-branches of the OH(3-1) and OH(4-2) bands are included in the data and integrated branch

intensities are available for these emissions. Figure 1 displays a typical spectrum acquired with an exposure time of 15 seconds by the GRIPS 9 instrument. The shaded areas denote those parts of the spectrum which are taken as best estimates for the Q-branch intensities. The high temporal resolution and the fact that both emissions are imaged onto the sensor area at the same time make the GRIPS instruments well-suited for the intended analysis. The instrument GRIPS 6 has been in operation at the NDMC site Oberpfaffenhofen, Germany, since January 2009. Technical details as well as the processing scheme of the data are described by Schmidt et al. (2013). GRIPS 9 was operated at the Arctic Lidar Observatory for Middle Atmosphere Research (ALOMAR), Norway, from November 2010 until May 2014. Both technically identical instruments point to the zenith with an effective field of view (FOV) that corresponds to ca. 24 km x 24 km at the altitude of 87 km.

The TANGOO instrument measures the OH(6-2) and O_2b(0-1) emissions, covering the spectral range between 839 nm and 867 nm. Its interference filter (manufactured by Andover Corporation) has a central wavelength of 867.1 nm with a full width at half maximum (FWHM) of 0.97 nm and a free aperture of 110 mm. The wavelength is continuously scanned by tilting the filter mounted in a thermally isolated chamber and the signal itself is recorded with a Hamamatsu Photonics R943-02 photomultiplier tube operated in photon counting mode. Thus, there is a time difference between the registration of the OH(6-2) and O_2b(0-1) emissions of approximately one minute. TANGOO is based on the successful experience with the Argentine Airglow Spectrometer presented by Scheer (1987), which has been acquiring data for many years so far.

With 0.4° x 2.0°, the TANGOO FOV is almost two orders of magnitude smaller than that of GRIPS 6, providing a considerably higher sensitivity to small scale structures. Despite this large difference in the FOV size, usually no significant differences are observed on the time scales relevant for this study (>0.5 h). For the GRIPS, a detailed discussion of observational

selection concerning vertical and horizontal wavelengths was recently given by Wüst et al. (2016). TANGOO was developed at the German Aerospace Center (DLR) in close cooperation with IAFE/CONICET (Instituto de Astronomía y Física del Espacio, Consejo Nacional de Investigaciones Científicas y Técnicas) and started routine operations at Oberpfaffenhofen, Germany, in March 2013. Since TANGOO was temporarily deployed at another NDMC site, only 25 months with 161 cloudless nights of parallel observations between the two airglow spectrometers are available for this study.

2.2 ALOMAR Weber Na Lidar

The sodium lidar at ALOMAR is capable of measuring sodium density, temperatures and wind in the height region from 70 km to 110 km - the height range of the upper mesospheric sodium layer (peak height: ~92 km). It was deployed in August 2000 and during the time interval of interest for this study it was operated in the configuration described by Dunker et al. (2013). With an aperture of only 0.6 mrad its FOV in the MLT region is on the order of <100 m. Unlike the airglow spectrometers used in this study, the two beams of the lidar usually do not point into zenith direction. In order to retrieve wind velocity one beam usually points 20° to the north and the other 20° to the east. Thus, the FOV of the Na lidar and GRIPS are close to each other but do not overlap. Figure 2 illustrates the temporal evolution of the temperature profiles of the two beams during the night of January 21/22, 2012. As to be expected only small differences are visible. These can be attributed to the separation of their FOV, which amounts to about 65 km at the peak height of the Na layer (ca. 92 km).

3 Results and discussion

3.1 GRIPS 9 versus the ALOMAR Na lidar

As mentioned above, the GRIPS 9 instrument was operated at ALOMAR during four winter seasons from November 2010 until May 2014. During the long winter nights at these high latitudes (69° N) it is evident that the individual OH branches show small differences in reaction to dynamical disturbances. Figure 3a) depicts the relative intensity perturbations of the OH(3-1) Q-branch (black) and the OH(4-2) Q-branch (grey) observed during the night of January 21/ 22, 2012 (corresponding to the lidar measurements shown in Figure 2). The scale refers to the change with respect to the nightly mean, 0.1 representing 10 % deviation. During phases of decreasing intensity the OH(3-1) intensity appears to lie systematically above the OH(4-2) intensity, e.g., between 18 UT and 20 UT or 0:30 UT and 2 UT; the opposite is the case for phases of increasing intensities, e.g., between 4 UT and 6 UT. Since these differences are not symmetric about the times of maximum (minimum) intensities, they are not simply due to different amplitudes in the two emissions but reflect a small phase shift in the temporal evolution of the oscillations. This interpretation is supported by the result of the harmonic analysis (HA) also displayed in the Figure. The HA performs a least squares fit, but is used here in the implementation described by Bittner et al. (1994), which is able to identify a single period, minimizing the residuals in two independent time series. This allows investigating potential changes in amplitude and phase between the two data sets. Subsets 3b) and 3c) illustrate the results for the second and third oscillation identified in the data.

The phase differences for the 3.0 h and 6.9 h oscillations are well defined, while for the 15.9 h oscillation it is negligible. The intensity ratio of the two emissions is of interest, because it highlights systematic differences between the two emissions more clearly. Apparently, the intensity of the OH(4-2)-emission is on average 30 % larger than the OH(3-1)-emission intensity but their ratio also exhibits a significant variation with time (Figure 3d). Again dominant periods of 6.9 h and 3.2 h are identified with the HA also in the intensity ratios. Obviously, they agree well with those periods identified before, which exhibit a finite phase

199 difference (Figures 3a and 3c). Thus, the intensity ratios can be used to confirm the results of
200 the HA concerning potential phase differences of individual emissions.

201 As stated by Fagundes et al. (1995) in their comparison of the OI(557.7nm) and OH(9-4)
202 emission, a phase difference $\Delta\varphi$ is related to the vertical wavelength λ_z via the expression:

203 $$\lambda_z = \Delta h \frac{2\pi}{\Delta\varphi}. \quad (3.1)$$

204 In case of OH bands corresponding to adjacent upper vibrational levels, a first estimate of the
205 height difference Δh between the two layers can be adopted from von Savigny et al. (2012),
206 who derived an average of $\Delta h \approx 500$ m. With phase differences of 0.16 rad and 0.34 rad for the
207 3 h and 7 h period oscillations, the vertical wavelengths then amount to 19.4 km and 9.2 km.

208 These values agree well with the rough estimates derived by looking at the lidar profiles
209 shown in Figure 2. While in the lidar data the dominant wavelengths appear to change over
210 the night, the GRIPS analysis is based on the entire night. So in order to retrieve reliable
211 estimates for the dominant wavelengths in the lidar data, the HA is now applied to each lidar
212 profile individually. All data points with an uncertainty of more than ±10 K are omitted,
213 which limits the height range under investigation to approximately 80–105 km (without
214 setting fixed boundaries). Due to the limited height range and the typical temperature profile
215 with high temperatures at both the top (105 km) and the bottom (80 km), all wavelengths
216 greater than 40 km are excluded.

217 The retrieved dominant vertical wavelengths (black/grey) of two different nights are displayed
218 as a function of time in Figure 4 for both beams (solid/dashed). Subset 4a) again shows the
219 results for January 21/22, 2012. While the shorter wavelength (grey) exhibits little variation
220 throughout the night, the larger one (black) is not so constant. Until 22:00 UTC the results are
221 fairly stable yielding values between 25 km and 30 km; starting at 22:00 UTC the values

slowly decrease to smaller values around 20 km and increase again after 02:00 UTC, exhibiting a larger spread between 20 km and 40 km.

While the wavelengths retrieved for both beams agree fairly well for any given point in time, some uncertainty remains concerning how many different waves are actually present throughout the night. The following analysis is based on the minimum number of waves explaining the observations reasonable well (usually two) and attributing the remaining variability of the data to the uncertainty of the observations.

Thus, the mean dominant vertical wavelengths retrieved from the lidar profiles shown in Figures 2 and 4a) amount to 23.2 km ± 3.4 km and 11.5 km ± 1.2 km, with the individual values of beam 1 and its one-sigma interval being 23.1 km ± 5.3 km and 11.6 km ± 1.8 km (23.3 km ± 4.2 km and 11.4 km ± 1.6 km for beam 2). Depending on the signal-to-noise ratio and the actual atmospheric conditions the retrieved values exhibit a higher or lower variability. Figure 4b) shows an example with higher variability during the first half of the night (due to a smaller signal-to-noise ratio) and fairly constant values during the second half of the night.

Although GRIPS is only operated during night time (winter) and only nights with excellent observing conditions are incorporated in the analysis, we have still succeeded in identifying 24 wave events in 22 nights. At least two waves are identified in any of the lidar observations analyzed here, but only one vertical wavelength can usually be retrieved from the GRIPS data.

The calculation of the uncertainty of the wavelengths measured by lidar has already been described above. In the case of GRIPS, the uncertainties of Δh and $\Delta\varphi$ in eq. (3.1) contribute to the overall uncertainty. Dealing with $\Delta(\Delta\varphi)$, the uncertainty of $\Delta\varphi$, is not as trivial as one might think, as standard methods appear to overestimate it: despite the ratio OH(3-1)/OH(4-2)

often undoubtedly indicating non-zero values of the phase shift $\Delta\varphi$, calculations may still show $\Delta\varphi \approx 0$ within numerical precision. Similar difficulties arise in case of the height separation uncertainty $\Delta(\Delta h)$, because the value of $\Delta h = 500$ m adopted from von Savigny et al. (2012) is only a statistical mean and individual observations may differ substantially from this value.

Therefore, several selection criteria are applied to the results of the spectral analysis, which are: (1) similar periods need to be identified in both the OH(3-1), OH(4-2) intensities as well as in their ratio, (2) the relative amplitude of the oscillation of the intensity ratios must at least amount to one percent, (3) a minimum phase shift $\Delta\varphi$ of 0.1 rad between the OH(3-1) and OH(4-2) intensities is required. This ensures that $\Delta(\Delta\varphi)$ is small and the overall uncertainty can be attributed to the unknown value of $\Delta(\Delta h)$. The calculation of λ_z is now repeated for different values of the height separation Δh in order to exactly match the results retrieved from the lidar observations for the entire data set.

The results indicate that Δh has to vary from 260 m to 860 m for a perfect agreement between the two systems, with a mean $\Delta h = 540$ m, $1\sigma = 160$ m, but 95 % of the values already lying within 540 m ± 240 m. $\Delta h = 540 \text{ m} \pm 1\sigma$ is adopted for all values stated in this study (unless stated otherwise). It should be noted, that this is only an upper limit for the uncertainty of Δh, since it includes contributions from $\Delta(\Delta\varphi)$, which were neglected here and for simplicity we assume that the vertical wavelength from the lidar has no systematic or statistical error. However, this approach yields a reasonable estimate of the overall uncertainty, so that λ_z can be determined with a precision of ± 30 %. Figure 5 shows a scatter plot of the wavelengths retrieved from GRIPS versus the Na lidar wavelengths showing that the wavelengths of 18 out of the 24 wave events agree within their confidence intervals.

3.2 GRIPS 6 versus TANGOO

For 25 months between March 2013 and July 2016, the TANGOO airglow spectrometer observed the OH(6-2) and O_2b(0-1) bands co-located with GRIPS 6 at Oberpfaffenhofen. Vertical wavelengths retrieved from the phase shift between oscillations in the OH and O_2 intensities provide independent evidence, which can serve for validation of the OH(3-1)/OH(4-2) approach. During the night of July 27/28, 2013 the TANGOO data show a distinct phase shift of nearly $\pi/2$ between the O_2 and the OH(6-2) intensity variations (Fig. 6a). The observed amplitudes agree well in spite of the differences between the two instruments, especially the horizontal extents of their FOV (Fig. 6b). A phase shift between the OH emissions is not obvious, but the OH(3-1)/OH(4-2) ratio again exhibits a similar variation as the intensities themselves (Fig. 6c). The maxima of the ratios (dashed vertical lines) coincide with decreasing intensities; minima correspond to increasing intensities but not as clearly. This indicates that the variation is not simply caused by clouds, which would make the intensities and their ratios vary in phase.

Vertical wavelengths can be determined according to eq. (3.1) for both data sets. While Δh=540 m ±160 m for GRIPS 6 can be adopted from section 3.1, many studies dealing with simultaneous observations of OH and O_2 emissions work with typical centroid heights of 87 km and 95 km. However, as pointed out by Liu and Swenson (2003) and by Vargas et al. (2007), this separation of approximately 8 km may be significantly reduced to between 5.1 km and 5.6 km because of the gravity-wave-induced perturbation of the emission profiles. Therefore, we adopt a mean separation of 5.5 km between OH(6-2) und O_2. This is approximately the upper value proposed by the above-mentioned authors but still significantly smaller than the common 8 km. For the prominent period of 1.1 h shown in Figure 6, wavelengths of 18.5 km ± 5.5 km (GRIPS) and 13.2 km (TANGOO) are obtained in this way (19.2 km instead of 13.2 km if 8 km separation are adopted for the TANGOO observations).

Such a comparison is done for the entire available data set of 161 nights that pass the data quality criteria. With the HA, 233 waves were identified and wavelength derivation according to the criteria outlined above was initially possible for 136 waves. The other events had to be excluded, mostly due to insignificant phase differences or small amplitudes. Another 34 events were excluded due to large uncertainties of the retrieved values caused by the 2π ambiguity in eq. (3.1): the phase shift between the OH and O_2 intensities may be interpreted as $\Delta\varphi$ or $\Delta\varphi \pm 2\pi$, $\pm 4\pi$ etc. (especially ambiguous, when $|\Delta\varphi|$ approaches π). It should be noted that in all these events waves are clearly present, but their parameters cannot be precisely determined. This $\pm 2\pi$ ambiguity is irrelevant when only the small $\Delta\varphi$ between different OH emissions are considered, but in case of OH and O_2, $\Delta\varphi$ can become considerably larger. Excluding ambiguous values from the analysis effectively limits the vertical wavelengths under investigation to approximately 5 km – 40 km. This is only a minor limitation, since shorter wavelengths are not supposed to be observable at all due to the finite widths of the emission layers and the rather small $\Delta\varphi$ of larger wavelengths are neither resolved by the temporal resolution nor can they be distinguished from the case of ducting or evanescence.

According to the criteria discussed above, the determination of λ_z is accepted for periods below 4 h in two-thirds of the cases, but for periods above 6 h results are only accepted for a quarter of the cases. Figure 7a) illustrates this dependence on wave period for all 233 waves observed, discriminating between accepted (black) and rejected (grey) λ_z. This may be one of the reasons why Wrasse et al. (2004) did not find any significant phase shift between the OH(6-2) and OH(8-3) emission in their 19 nights of observation.

The mean wavelength of the 102 cases retrieved from the OH(3-1)/OH(4-2) comparison is 22.9 km (1-σ: 9.0 km) with the median being 22.7 km. The respective values based on the OH(6-2)/O_2 comparison are 19.1 km mean wavelength (1-σ: 8.9 km) and 18.4 km for the median. The mean ratio of the wavelengths determined from the two instruments amounts to

0.99, the median is 0.83 (Figure 7 b)). This indicates that the apparent wavelengths of the OH(6-2) vs. O_2 analysis are on average shorter by roughly 20 % compared to the OH(3-1) vs. OH(4-2) analysis. The mean difference and the wide distribution can be explained by the assumptions made for Δh. Both a reduction to 450 m for the height separation between the individual OH vibrational transitions and an increase to 6.5 km concerning the separation between OH(6-2) and O_2 lead to a more consistent median. The latter value of 6.5 km however is in better agreement with the nominal height separation of 7 km to 8 km. It is important to note that the height separation between all the emissions used here is actually a statistical relationship, and individual values may indeed vary a lot across a larger data set of many nights. The recent study by Teiser and von Savigny (2017) gives a comprehensive overview of the variability of the OH(3-1) and OH(6-2) emission altitudes based on SCIAMACHY data for a fixed local time.

In order to better understand the larger scatter of the wavelengths obtained by the two airglow spectrometers (Figure 7b)) in contrast to the rather good agreement achieved in the OH / Na-lidar comparison (Figure 5), another five nights with different types of oscillations are shown in Figure 8. In each case, periods and phases were obtained by the HA as shown in Figure 3 but have been omitted in the plot. Figure 8a) shows one of the clear cases, in which a 3.3 h period is clearly visible in all four emissions and well reproduced by the HA with a distinct phase shift, confirmed also by the OH(3-1)/OH(4-2) ratio. The corresponding wavelengths of 18.7 km (GRIPS) and 22.3 km (TANGOO) agree fairly well in this case. The second example (8b) shows the only case in the entire data set, for which an apparent upward propagating phase was determined for a long period oscillation of approximately 7 h. This case meets all the criteria outlined above and both observations yield wavelengths of -14.5 km (GRIPS) and -19.0 km (TANGOO), the negative sign indicating upward phase propagation. An alternative explanation may be a horizontal wind larger than and opposite to the horizontal phase speed of the wave. Although upward propagating waves (with downward phase progression) are

346 expected to dominate the spectrum at ca. 90 km height (see review by Fritts and Alexander,
347 2003). Only one wave in our data set shows downward propagation, which is consistent with
348 this view, but smaller than the notable percentage reported by Reisin and Scheer (2001). This
349 may not be a serious discrepancy, given a possible selectivity of our present approach and the
350 complicated processes involved in wave reflection (e.g., Wüst and Bittner, 2008). At the
351 beginning of the night shown in Figure 8c) a small shift between OH and O_2 is apparent
352 (20:30 UT until 21:00 UT), but during the times of maximum amplitudes at 23:00 UT it again
353 increases to about π. Clearly, more than one wave is present during this night and it is difficult
354 to retrieve reliable estimates for the phases of the individual oscillations (compare also the
355 OH(3-1)/OH(4-2) ratio, showing different behavior than the emissions themselves). Thus,
356 only a short period (1.6 h) oscillation matches the analysis criteria with vertical wavelengths
357 of 24.7 km (GRIPS) and 18.3 km (TANGOO). Figure 8d) shows an example in which the OH
358 and O_2 emissions behave differently after 01:30 UT (an uncommon case). Despite some
359 oscillations clearly visible in the OH(3-1)/OH(4-2) ratio, the phase shift could not be derived
360 reliably. The same applies to an example of the most common type of nights excluded from
361 analysis (Figure 8e)). Despite the phase shift clearly visible, especially after 20:00 UT and in
362 the OH(3-1)/OH(4-2) ratio, the overlying long-period oscillation (or slope) prevents
363 calculating a reliable quantitative estimate for $\Delta\varphi$. About half of the nights had to be excluded
364 either because of small phase shifts in the order of the measurement uncertainty or because of
365 an overlying long-period oscillation / slope of this kind.

366 In principle the values of λ_z can be entered into the dispersion relation for gravity waves to
367 retrieve the corresponding horizontal wavelengths λ_h. Then, if reasonable assumptions are
368 made for the Brunt-Väisälä frequency (0.02 rad/s^{-1}) and for the range of the horizontal winds
369 (up to ±80m/s), estimates for the energy density of the waves can be calculated (e.g., Wüst et
370 al., 2016; Wüst et al., 2017b). But with the given uncertainty of the estimates for the winds
371 and λ_z the final results (not shown) also have a considerable uncertainty. The calculations

372 indicate that the waves have horizontal wavelengths between approximately 100 km and
373 1000 km and fall mostly into the mesoscale range. It follows that the waves under
374 consideration in this study belong to a type which is rather common in the canonical gravity
375 wave spectrum, because both the horizontal wave number k as well as the angular frequency
376 ω are small (see, e.g., Fritts and Hoppe, 1995).

377

378 **4 Summary and Conclusions**

379 Integrated intensities of the OH(3-1) and OH(4-2) Q-branch were extracted from GRIPS
380 airglow spectrometers acquiring data in the spectral range between 1.5 µm and 1.6 µm. Their
381 time series often exhibit small phase shifts, which can be attributed to the presence of
382 atmospheric waves. These waves influence the individual vibrational transitions – originating
383 from different altitudes – at different times. The estimated phase shifts were successfully used
384 to derive wave parameters.

385 The validity of the retrieval technique was tested by comparing GRIPS 9 airglow observations
386 with the co-located sodium lidar at ALOMAR (69.28° N, 16.01° E). Best agreement between
387 the two data sets is achieved if a mean height difference of 540 m (1σ = 160 m) is assumed
388 for the emission heights between the centroid heights of the OH bands from neighboring
389 upper vibrational levels. This is in reasonable agreement with the estimate of 500 m obtained
390 by von Savigny et al. (2012) from satellite observations and modelling.

391 A large data set of 161 nights acquired with the GRIPS 6 instrument at Oberpfaffenhofen
392 (48.08° N, 11.27° E) was compared to the co-located TANGOO spectrometer observing the
393 OH(6-2) and O_2b(0-1) emissions. The 102 wavelengths successfully derived from both data
394 sets have a larger scatter compared to the GRIPS-lidar intercomparison. This can be attributed
395 to the assumptions made for the height separation between the individual emissions. They

tend to agree best, if the same centroid height separation as from the ALOMAR comparison is assumed in case of OH(3-1) vs. OH(4-2) and 6.5 km in case of OH(6-2) vs. O_2b(0-1). Since these values are statistical means, individual cases may differ substantially, explaining the variance of the results. The mean wavelength determined from the OH(3-1) vs. OH(4-2) relationship is 22.9 km (1-σ: 9.0 km).

Despite the large difference in the FOV of GRIPS 6 and TANGOO, no significant differences between the two data sets are observed on the time scales relevant for this study (>0.5 h), which can be deduced from the identical OH amplitudes recorded by the two instruments. Therefore, we conclude that observational selection is most likely caused by the finite OH layer width (ca. 8–10 km) rather than the FOV.

The retrieval based on the comparison of OH(3-1) and OH(4-2) is more successful for periods below 4 hours, which may be due to the larger relative phase differences in case of shorter periods and/or due to a higher fraction of tidal waves with different physical properties in the longer period range. More than 16 instruments, largely identical to our GRIPS, are currently operated by different investigators throughout the NDMC. Thus, this approach appears to be feasible for estimating latitudinal and longitudinal differences in the vertical wavelength spectra.

Currently, we are performing first observations with a new instrument, observing not only the OH(3-1) and OH(4-2) transitions but also OH(7-4) and OH(8-5). The combination of several transitions is intended to further improve the precision of the retrieved vertical wavelengths.

Acknowledgements

419 The airglow observations at ALOMAR were partly funded by the Bavarian State Ministry for
420 Environment and Consumer Protection [project BHEA, grant number TLK01U-49580]. The
421 lidar observations and analysis were funded by the Research Council of Norway through
422 grants 216870/F50 and 208020/F50. The ALOMAR Na lidar was a National Science
423 Foundation Upper Atmosphere Facility instrument, funded under grant NSF AGS-1136269.
424

425 **References**

426

427 Baker, D. J., Stair Jr., A.T., 1988. Rocket measurements of the altitude distributions of the
428 hydroxyl airglow. Physica Scripta 37 (4), 611–622, http://dx.doi.org/10.1088/0031-
429 8949/37/4/021.

430

431 Beig, G., Keckhut, P., Lowe, R. P., Roble, R. G., Mlynczak, M. G., Scheer, J., Fomichev, V.
432 I., Offermann, D., French, W. J. R., Shepherd, M. G., Semenov, A. I., Remsberg, E. E., She,
433 C. Y., Lübken, F. J., Bremer, J., Clemesha, B. R., Stegman, J., Sigernes, F., Fadnavis, S.,
434 2003. Review of mesospheric temperature trends. Reviews of Geophysics, 41 (4), 1015–1055,
435 http://dx.doi.org/10.1029/2002RG000121.

436

437 Bittner, M., Offermann, D., Bugaeva, I.V., Kokin, G.A., Koshelikov, J.P., Krivolutsky, A.,
438 Tarasenko, D.A. , Gil-Ojeda, M., Hauchecorne, A., Lübken, F.-J., de la Morena, B.A.,
439 Mourier, A., Nakane, H., Oyama, K.I., Schmidlin, F.J., Souble, I., Thomas, L., Tsuda, T.,
440 1994. Long period/ large scale oscillations of temperature during the DYANA campaign. J.
441 Atmos. Terr. Phys. 56 (13/14), 1675-1700, http://dx.doi.org/10.1016/0021-9169(94)90004-3.

442

443 Bittner M., Offermann, D. Graef, H.H., 2000. Mesopause temperature variability above a
444 midlatitude station in Europe. J. Geophys. Res. Atmos. 105 (D2), 2045-2058,
445 http://dx.doi.org/10.1029/1999JD900307.

446

447 Bittner M., Offermann, D., Graef, H.H., Donner, M., Hamilton, K., 2002. An 18 year time
448 series of OH rotational temperatures and middle atmosphere decadal variations. J. Atmos.
449 Terr. Phys. 64 (8-11), 1147-1166, http://dx.doi.org/10.1016/S1364-6826(02)00065-2.

450

451 Dunker, T., Hoppe, U. P., Stober, G., Rapp, M., 2013. Development of the mesospheric Na
452 layer at 69° N during the Geminids meteor shower 2010. Ann. Geophys. 31, 61-73,
453 http://dx.doi.org/10.5194/angeo-31-61-2013.

454

455 Fagundes, P. R., Takahashi, H., Sahai, Y., Gobbi, D., 1995. Observations of gravity waves
456 from multispectral mesospheric nightglow emissions observed at 23° S. J. Atmos. Terr. Phys.
457 57 (4), 395-405, http://dx.doi.org/10.1016/0021-9169(94)E0007-A.

458

459 French, W.J.R., Klekociuk, A.R., 2011. Long-term trends in Antarctic winter hydroxyl
460 temperatures. J. Geophys. Res. Atmos. 116 (D4), http://dx.doi.org/10.1029/2011JD015731.

461

462 Fritts, D. C., Alexander, M. J., 2003. Gravity wave dynamics and effects in the middle
463 atmosphere. Reviews of Geophysics, 41 (1), http://dx.doi.org/10.1029/2001RG00D106.

464

Fritts, D.C., Hoppe, U.-P., 1995. High-resolution measurements of vertical velocity with the European incoherent scatter VHF radar 2. Spectral observations and model comparisons. J. Geophys. Res. Atmos. 100 (D8), 16827-16838, http://dx.doi.org/10.1029/95JD01467.

Guharay, A., Taori, A., Taylor, M., 2009. Summer-time nocturnal wave characteristics in mesospheric OH and O_2 airglow emissions. Earth Planets Space 60 (9), 973–979, http://dx.doi.org/10.1186/BF03352853.

Hannawald, P., Schmidt, C., Wüst, S., Bittner, M., 2016. A fast SWIR imager for observations of transient features in OH airglow. Atmos. Meas. Tech. 9 (4), 1461-1472, http://dx.doi.org/10.5194/amt-9-1461-2016.

Hines, C.O., Tarasick, D.W., 1987. On the detection and utilization of gravity waves in airglow studies. Planet. Space Sci. 35, 851-866, http://dx.doi.org/10.1016/0032-0633(87)90063-8.

Liu, A.Z., Swenson, G.R., 2003. A modeling study of O2 and OH airglow perturbations induced by atmospheric gravity waves. J. Geophys. Res. 108 (D4), 4151, http://dx.doi.org/10.1029/2002JD002474.

López-González, M. J., Rodríguez, E., ., Shepherd, G. G., Sargoytchev, S., Shepherd, M. G., Aushev, V. M., Brown, S., García-Comas, M., Wiens, R.H., 2005. Tidal variations of O_2 Atmospheric and OH (6-2) airglow and temperature at mid-latitudes from SATI observations. Ann. Geophys. 23 (12), 3579–3590, http://dx.doi.org/10.5194/angeo-23-3579-2005.

López-Moreno, J. J., Rodrigo, R., Moreno, F., López-Puertas, M., A. Molina, A., 1987. Altitude distribution of vibrationally excited states of atmospheric hydroxyl at levels v = 2 to v = 7. Planet. Space Sci. 35 (8), 1029-1038, http://dx.doi.org/10.1016/0032-0633(87)90007-9.

Perminov, V.I., Semenov, A.I., Medvedeva, I.V., Zheleznov, Y.A., 2014. Variability of mesopause temperature from the hydroxyl airglow observations over mid-latitudinal sites, Zvenigorod and Tory, Russia. Adv. Space Res. 54 (12), 2511-2517, http://dx.doi.org/10.1016/j.asr.2014.01.027.

Reisin, E.R., Scheer, J., 1996. Characteristics of atmospheric waves in the tidal period range derived from zenith observations of O_2(0-1) Atmospheric and OH(6-2) airglow at lower midlatitudes. J. Geophys. Res. 101, 21223-21232, http://dx.doi.org/10.1029/96JD01723.

Reisin E.R., Scheer, J., 2001. Vertical propagation of gravity waves determined from zenith observations of airglow. Adv. Space Res. 27 (10), 1743-1748, http://dx.doi.org/10.1016/S0273-1177(01)00313-1.

Scheer, J., 1987. Programmable tilting filter spectrometer for studying gravity waves in the upper atmosphere. Applied Optics 26 (15), 3077-3082, http://dx.doi.org/10.1364/AO.26.003077.

511 Schmidt, C., K. Höppner, Bittner, M., 2013, A ground-based spectrometer equipped with an
512 InGaAs array for routine observations of OH(3-1) rotational temperatures in the mesopause
513 region. J. Atmos. Sol. Terr. Phys. 102, 125-139, http://dx.doi.org/10.1016/j.jastp.2013.05.001.
514
515 Sedlak, R., Hannawald, P., Schmidt, C., Wüst, S., Bittner, M., 2016. High-resolution
516 observations of small-scale gravity waves and turbulence features in the OH airglow layer.
517 Atmos. Meas. Tech. 9 (12), 5955-5963, http://dx.doi.org/10.5194/amt-9-5955-2016.
518
519 Silber, I., Price, C., Schmidt, C., Wüst, S., Bittner, M., Pecora, E., 2017. First ground-based
520 observations of mesopause temperatures above the Eastern-Mediterranean Part I: Multi-day
521 oscillations and tides. J. Atmos. Sol. Terr. Phys. 155, 95-103,
522 http://dx.doi.org/10.1016/j.jastp.2016.08.014.
523
524 Swenson, G.R., Gardner, C.S., 1998. Analytical models for the responses of the mesospheric
525 OH* and Na layers to atmospheric gravity waves. J. Geophys. Res. Atmos. 103 (D6), 6271-
526 6294, http://dx.doi.org/10.1029/97JD02985.
527
528 Swenson, G. R., Liu, A.Z., 1998. A model for calculating acoustic gravity wave energy and
529 momentum flux in the mesosphere from OH airglow. Geophys. Res. Lett. 25 (4), 477-480,
530 http://dx.doi.org/10.1029/98GL00132.
531
532 Takahashi, H., Onohara, A., Shiokawa, K., Vargas, F., Gobbi, D., 2011. Atmospheric wave
533 induced O_2 and OH airglow intensity variations: effect of vertical wavelength and damping.
534 Ann. Geophys. 29 (4), 631-637, http://dx.doi.org/10.5194/angeo-29-631-2011.

Taori, A., Taylor, M. J., Franke, S., 2005. Terdiurnal wave signatures in the upper mesospheric temperature and their association with the wind fields at low latitudes (20° N). J. Geophys. Res. Atmos. 110 (D9), http://dx.doi.org/10.1029/2004JD004564.

Tarasick, D. W., Hines, C.O., 1990. The observable effects of gravity waves on airglow emissions. Planet. Space Sci. 38 (9), 1105-1119, http://dx.doi.org/10.1016/0032-0633(90)90019-M.

Teiser, G., von Savigny, Ch., 2017. Variability of OH(3-1) and OH(6-2) emission altitude and volume emission rate from 2003 to 2011. J. Atmos. Sol. Terr. Phys. 161, 28-42, http://dx.doi.org/10.1016/j.jastp.2017.04.010.

Vargas, F., Swenson, G., Liu, A., Gobbi, D., 2007. O (^{1}S), OH, and O_2(b) airglow layer perturbations due to AGWs and their implied effects on the atmosphere. J. Geophys. Res. Atmos. 112 (D14), http://dx.doi.org/10.1029/2006JD007642.

von Savigny, Ch., Lednyts' kyy, O., 2013. On the relationship between atomic oxygen and vertical shifts between OH Meinel bands originating from different vibrational levels. Geophys. Res. Lett. 40 (21), 5821-5825, http://dx.doi.org/10.1002/2013GL058017.

von Savigny, Ch., McDade, I. C., Eichmann, K. U., Burrows, J.P., 2012. On the dependence of the OH* Meinel emission altitude on vibrational level: SCIAMACHY observations and

558 model simulations. Atmos. Chem. Phys. 12 (18), 8813-8828, http://dx.doi.org/10.5194/acp-
559 12-8813-2012.

560

561 Wachter, P., Schmidt, C., Wüst, S., Bittner, M., 2015. Spatial gravity wave characteristics
562 obtained from multiple OH (3–1) airglow temperature time series. J. Atmos. Sol. Terr. Phys.
563 135, 192-201, http://dx.doi.org/10.1016/j.jastp.2015.11.008.

564

565 Wrasse, C. M., Takahashi, H., Gobbi, D., 2004. Comparison of the OH (8-3) and (6-2) band
566 rotational temperature of the mesospheric airglow emissions. Revista Brasileira de Geofísica
567 22 (3), 223-231, http://dx.doi.org/10.1590/S0102-261X2004000300002.

568

569 Wüst, S., Bittner, M., 2008. Gravity wave reflection: case study based on rocket data. J.
570 Atmos. Terr. Phys. 70, 742–755, http://dx.doi.org/10.1016/j.jastp.2007.10.010.

571

572 Wüst, S., Bittner, M., Yee, J.-H., Mlynczak, M.G., Russel III, J.M., 2017b. Variability of the
573 Brunt-Väisälä frequency at the OH*-layer height. Atmos. Meas. Tech. Discuss.,
574 http://dx.doi.org/10.5194/amt-2017-191, in review.

575

576 Wüst, S., Schmidt, C., Bittner, M., Silber, I., Price, C., Yee, J.-H., Mlynczak, M.G., Russel
577 III, J.M., 2017a. First ground-based observations of mesopause temperatures above the
578 Eastern-Mediterranean Part II: OH*-climatology and gravity wave activity. J. Atmos. Sol
579 Terr. Phys. 155, 104-111, http://dx.doi.org/10.1016/j.jastp.2017.01.003.

580

581 Wüst, S., Wendt, V., Schmidt, C., Lichtenstern, S., Bittner, M., Yee, J.H., Mlynczak, M.G.,
582 Russell III, J.M., 2016. Derivation of gravity wave potential energy density from NDMC
583 measurements. J. Atmos. Sol. Terr. Phys. 138-139, 32-46,
584 http://dx.doi.org/10.1016/j.jastp.2015.12.003.

585

586

587

588 **Figure captions**

589

590 Figure 1: Typical GRIPS 9 airglow spectrum. The shaded areas are taken as estimates for the
591 integrated intensities of the Q-branches (given in arbitrary units). They are acquired
592 simultaneously since the spectrum is imaged onto a 512-element InGaAs photodiode array.

593

594 Figure 2: ALOMAR Na lidar observations of January 21/22, 2012. The solid (dashed) lines
595 highlight the location of relative maxima (minima) in temperature. Similar structures with
596 vertical wavelengths of 10 km–15 km (thick lines, especially during the second half of the
597 night) or ca. 20 km (first half of the night: 10 km spacing between maximum and minimum
598 temperature) are observed in both beams.

599

600 Figure 3: a) relative intensity perturbation and successive harmonic fits (b) and c)), OH(3-1)
601 Q-branch intensity (grey), OH(4-2) Q-branch (black), same date as Figure 2. Small
602 differences between the two emissions exist and are highlighted by calculating their ratios
603 shown in subsets d) and e). Periods identified in the ratios match those periods found in the
604 emissions, which exhibit a distinct phase change.

605

606 Figure 4: The two dominant wavelengths retrieved from each lidar profile independently
607 throughout two different nights (solid and dashed: beam 1 and 2). The upper panel refers to
608 the night also shown in Figure 2. Nightly means (dots with error bars) and wavelengths
609 derived from the airglow observations (rectangles) are also shown.

610

611 Figure 5: Vertical wavelengths retrieved from the airglow observations versus those retrieved
612 from the lidar profiles. Only in two cases (grey triangles) more than one wavelength was
613 identified in the airglow data. The dashed grey line serves to guide the eye.

614

615 Figure 6: Airglow intensity variations displayed as relative deviation from the nightly mean
616 observed with a) the TANGOO instrument (green: O_2, red: OH(6-2)) and b) the GRIPS 6
617 (black: OH(3-1), blue: OH(4-2)). Also the ratio of the OH(3-1) and OH(4-2) intensities shown
618 in subset c) clearly shows systematic variability. The maxima of the ratios correspond to times
619 of declining intensities indicated by the dashed vertical lines.

620

621 Figure 7: The analysis yields reliable wavelength estimates predominantly for short period
622 waves (left panel). Comparison of the wavelengths independently retrieved from the OH(6-2)
623 and O_2 intensities with those retrieved from the OH(3-1) and OH(4-2) intensities (right panel).

624

625 Figure 8: Five nights (a-e) with different variability of the individual emissions. Upper
626 subpanels show OH(3-1) (black), OH(4-2) (blue), OH(6-2) (red) and O_2b(0-1) (green); lower
627 subpanels show the corresponding OH(3-1)/OH(4-2) ratio (black) with the dominant
628 oscillations retrieved by the harmonic analysis (red).

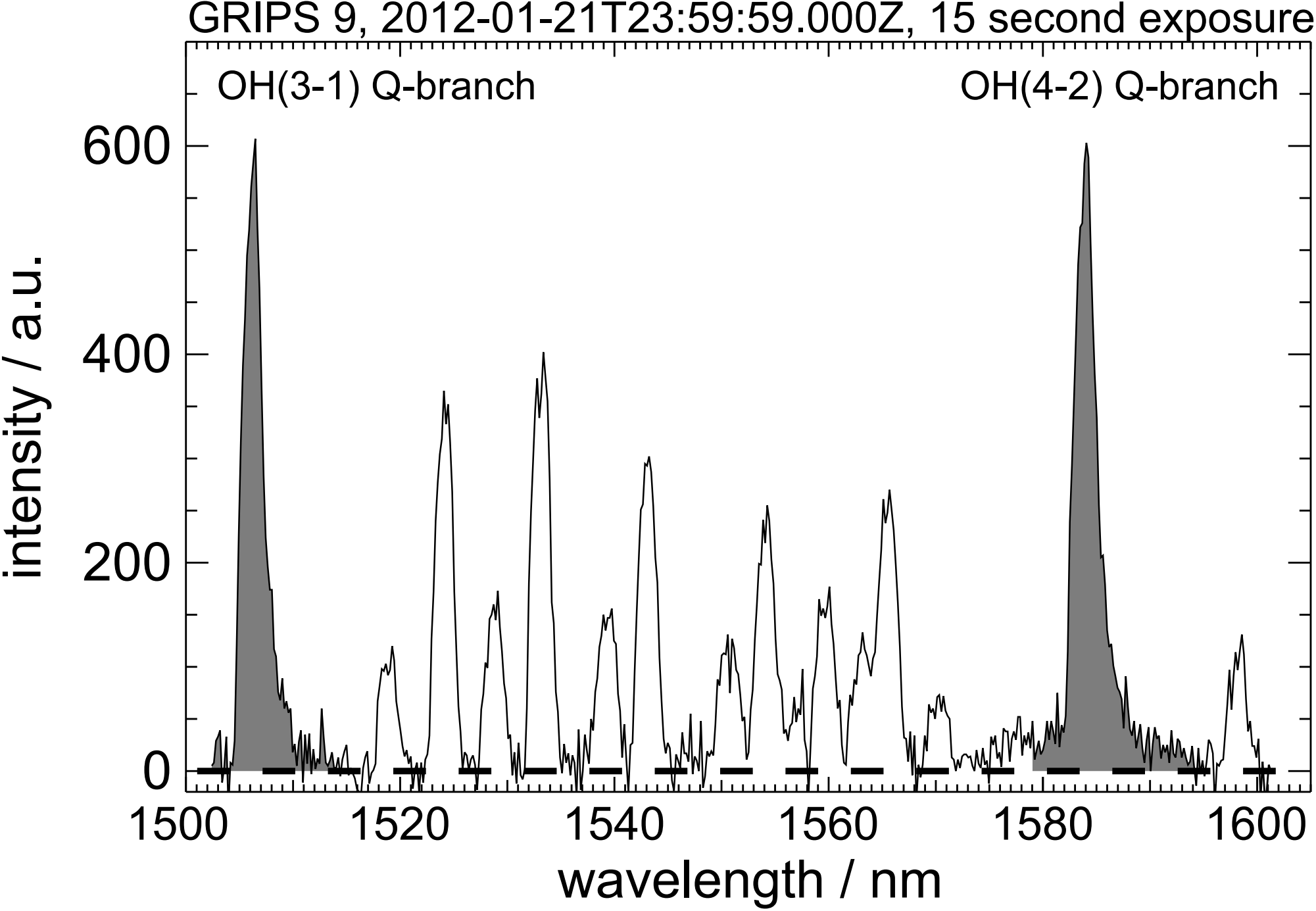
GRIPS 9, 2012-01-21T23:59:59.000Z, 15 second exposure
OH(3-1) Q-branch
OH(4-2) Q-branch
intensity / a.u.
0
200
400
600
1500
1520
1540
1560
1580
1600
wavelength / nm

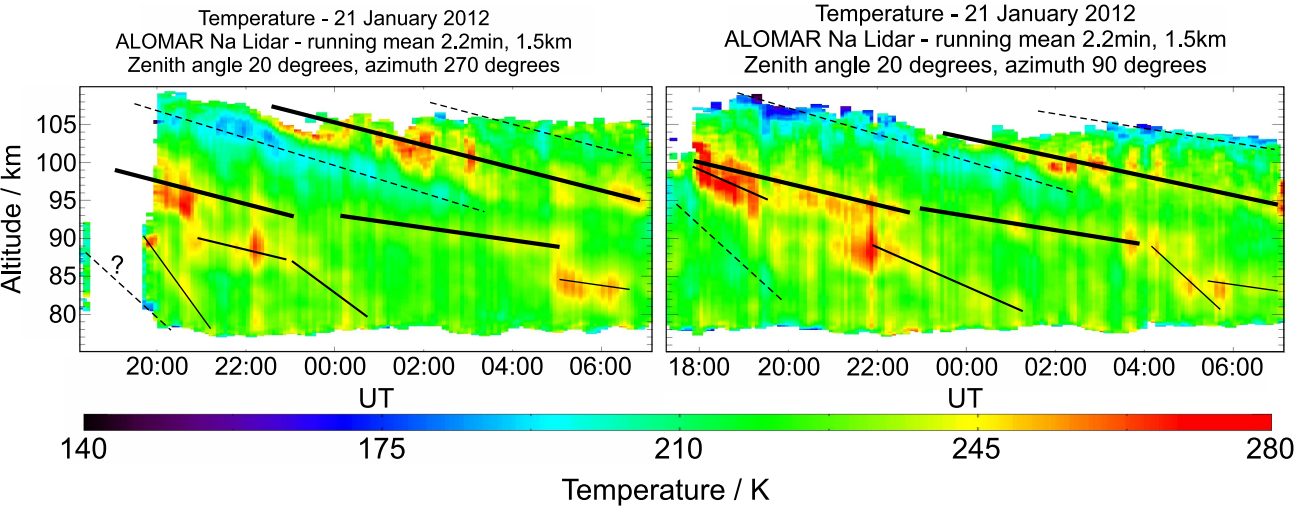
Temperature - 21 January 2012
ALOMAR Na Lidar - running mean 2.2min, 1.5km
Zenith angle 20 degrees, azimuth 270 degrees
Temperature - 21 January 2012
ALOMAR Na Lidar - running mean 2.2min, 1.5km
Zenith angle 20 degrees, azimuth 90 degrees
Altitude / km
105
100
95
90
85
80
?
20:00
22:00
00:00
02:00
04:00
06:00
UT
18:00
20:00
22:00
00:00
02:00
04:00
06:00
UT
140
175
210
245
280
Temperature / K

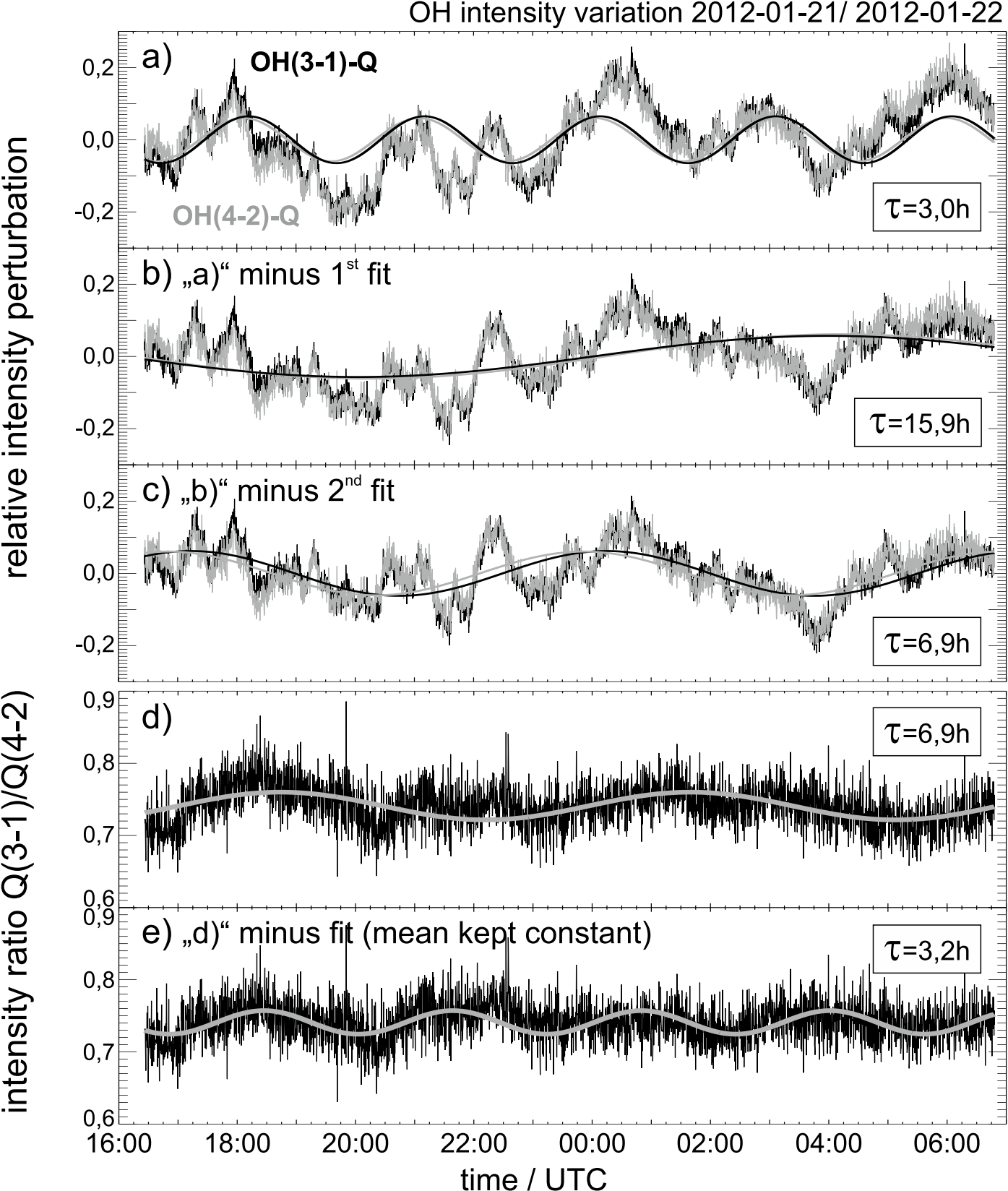
OH intensity variation 2012-01-21/ 2012-01-22
relative intensity perturbation
intensity ratio Q(3-1)/Q(4-2)
a)
OH(3-1)-Q
OH(4-2)-Q
τ=3,0h
b) „a)“ minus 1st fit
τ=15,9h
c) „b)“ minus 2nd fit
τ=6,9h
d)
τ=6,9h
e) „d)“ minus fit (mean kept constant)
τ=3,2h
0,2
0,0
-0,2
0,9
0,8
0,7
0,6
16:00
18:00
20:00
22:00
00:00
02:00
04:00
06:00
time / UTC

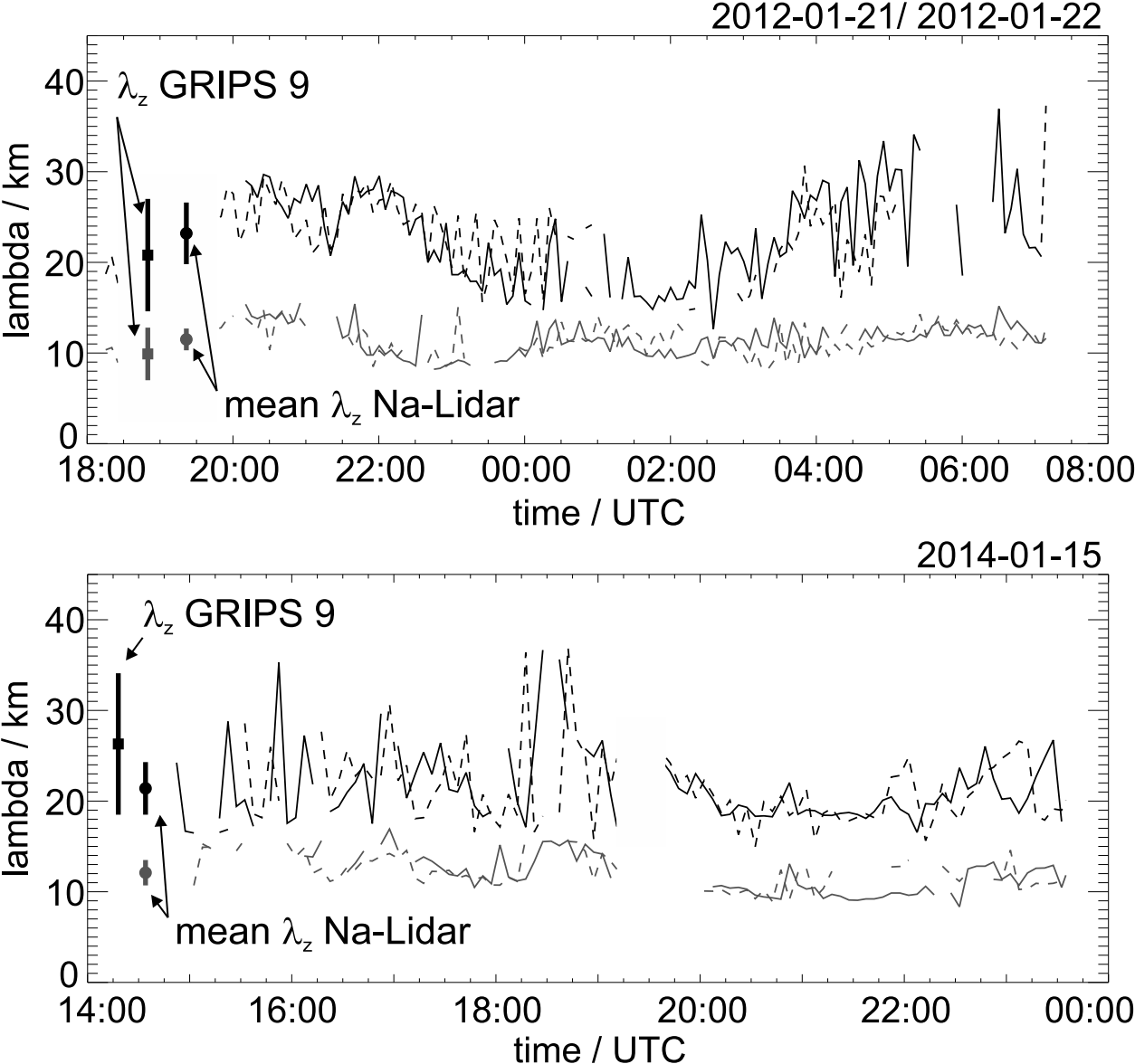
2012-01-21/ 2012-01-22
λz GRIPS 9
mean λz Na-Lidar
lambda / km
time / UTC
18:00
20:00
22:00
00:00
02:00
04:00
06:00
08:00
2014-01-15
λz GRIPS 9
mean λz Na-Lidar
lambda / km
time / UTC
14:00
16:00
18:00
20:00
22:00
00:00

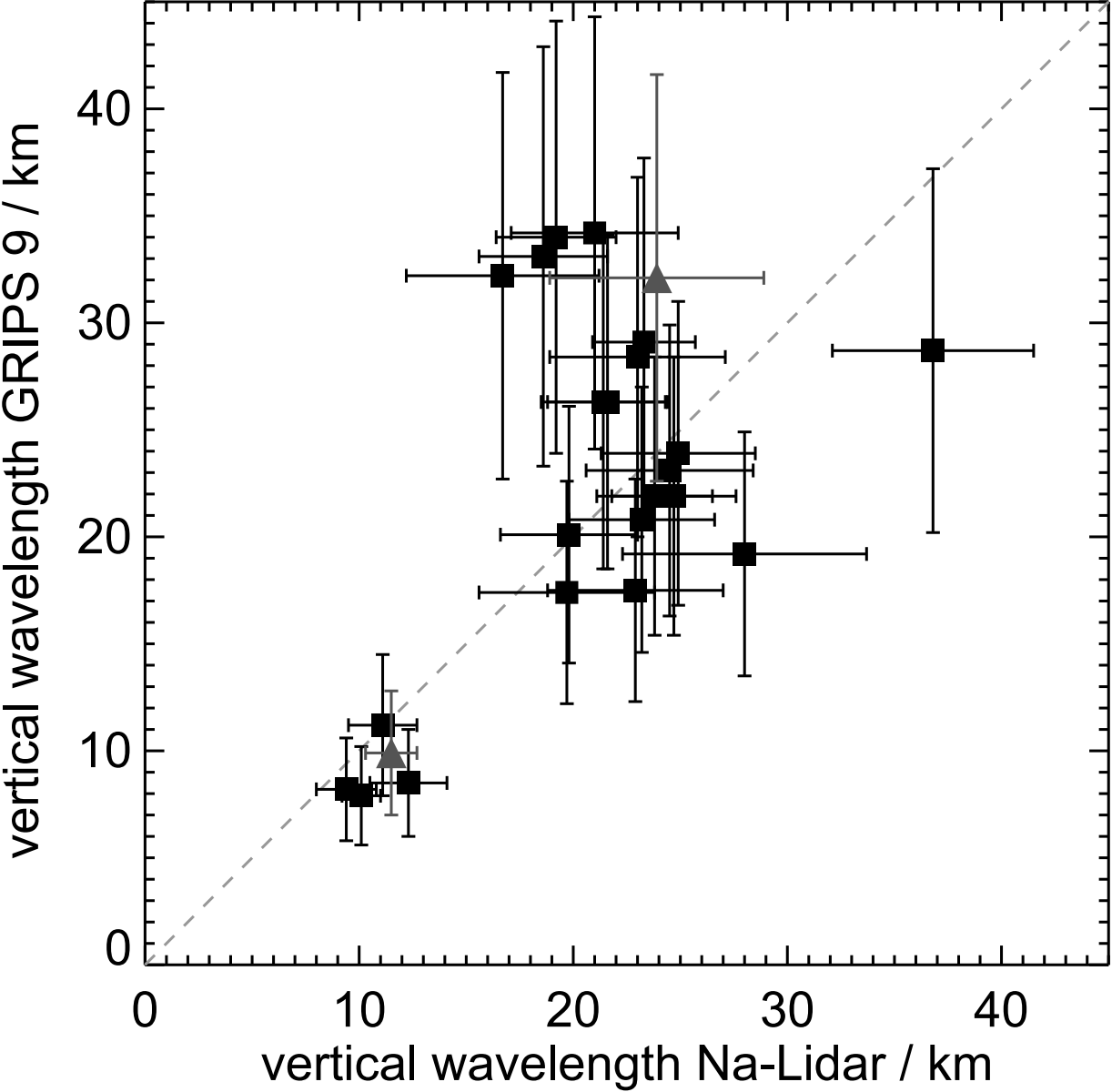
vertical wavelength GRIPS 9 / km
vertical wavelength Na-Lidar / km
0
10
20
30
40

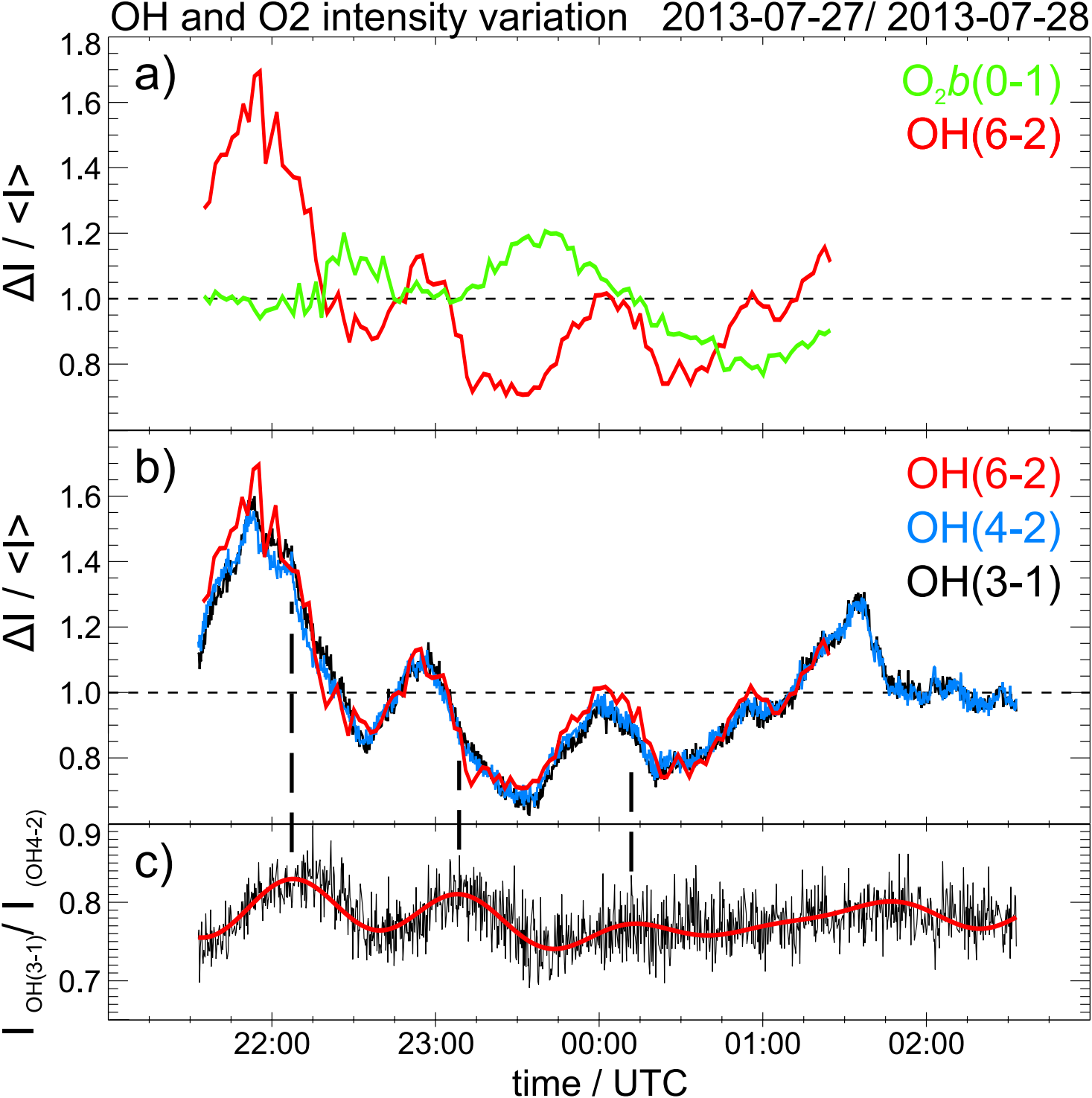
OH and O2 intensity variation 2013-07-27/ 2013-07-28
a)
O2b(0-1)
OH(6-2)
ΔI / <I>
b)
OH(6-2)
OH(4-2)
OH(3-1)
ΔI / <I>
c)
I OH(3-1)/ I (OH4-2)
22:00
23:00
00:00
01:00
02:00
time / UTC

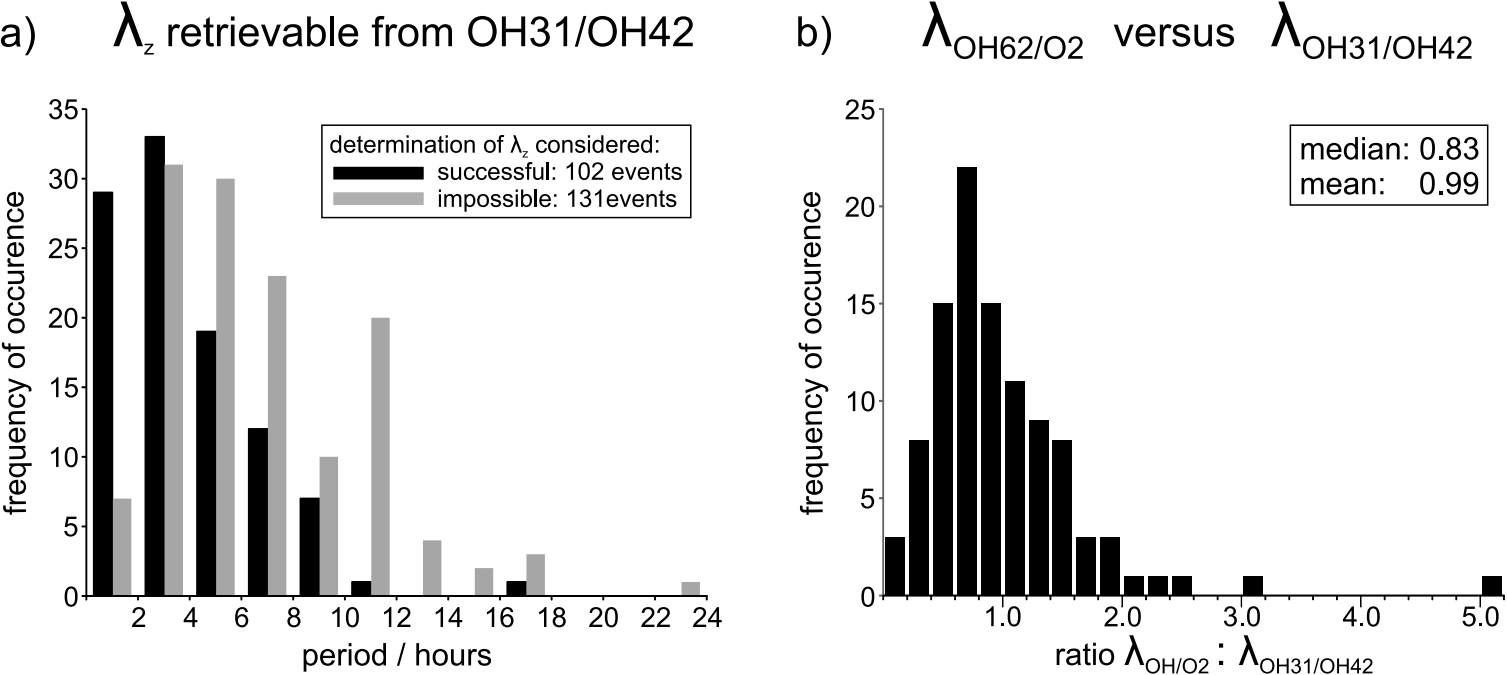
a)
λz retrievable from OH31/OH42
determination of λz considered:
successful: 102 events
impossible: 131events
frequency of occurence
period / hours
b)
λOH62/O2 versus λOH31/OH42
median: 0.83
mean: 0.99
frequency of occurence
ratio λOH/O2 : λOH31/OH42

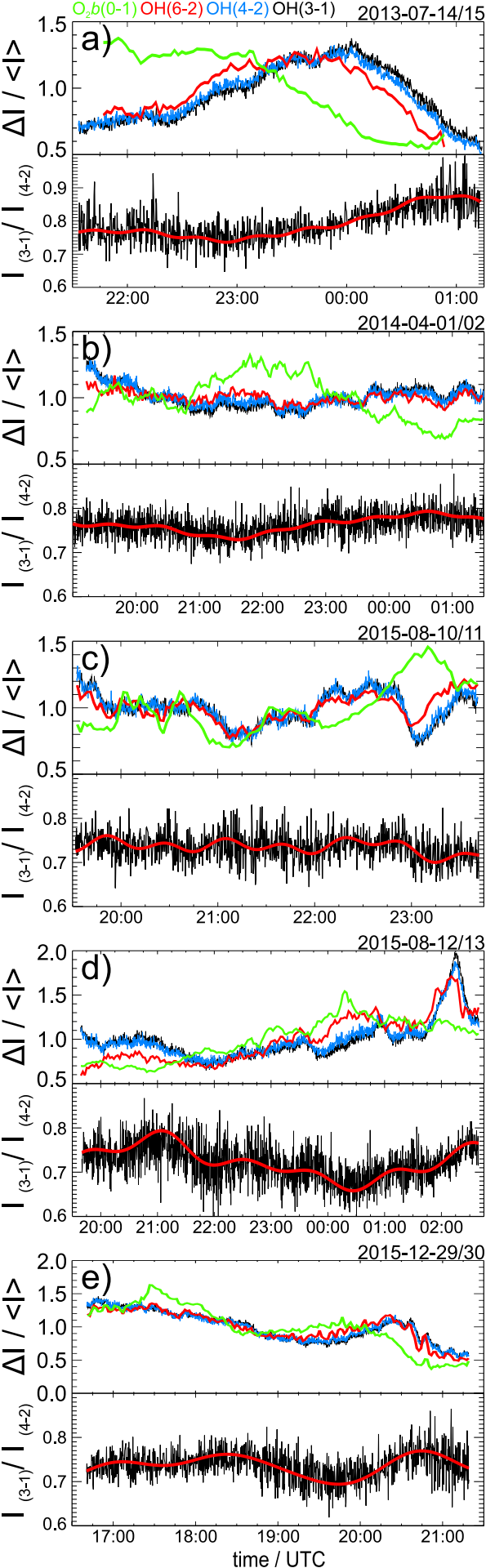
O2b(0-1) OH(6-2) OH(4-2) OH(3-1)
2013-07-14/15
a)
ΔI / <I>
I (3-1) / I (4-2)
22:00
23:00
00:00
01:00
2014-04-01/02
b)
20:00
21:00
22:00
23:00
00:00
01:00
2015-08-10/11
c)
20:00
21:00
22:00
23:00
2015-08-12/13
d)
20:00
21:00
22:00
23:00
00:00
01:00
02:00
2015-12-29/30
e)
17:00
18:00
19:00
20:00
21:00
time / UTC